HHS Public Access

Author manuscript

Mol Cancer Res. Author manuscript; available in PMC 2020 March 01.

Published in final edited form as:

Mol Cancer Res. 2019 September ; 17(9): 1842–1853. doi:10.1158/1541-7786.MCR-19-0257.

Identification of targetable recurrent MAP3K8 rearrangements in melanomas lacking known driver mutations

Brian D. Lehmann[1,*], **Timothy M. Shaver**[1], **Douglas B. Johnson**[2], **Zhu Li**[1], **Paula I. Gonzalez-Ericsson**[3], **Violeta Sánchez**[4], **Yu Shyr**[5], **Melinda E. Sanders**[3], **Jennifer A. Pietenpol**[1]

[1]Department of Biochemistry, Vanderbilt University, Nashville, TN, USA

[2]Department of Medicine, Vanderbilt University School of Medicine, Nashville, TN, USA

[3]Department of Pathology, Vanderbilt University School of Medicine, Nashville, TN, USA

[4]Department of Medicine, Vanderbilt University School of Medicine, Nashville, TN, USA

[5]Center for Quantitative Sciences, Vanderbilt University School of Medicine, Nashville, TN, USA

Abstract

Melanomas are characterized by driver and loss-of-function mutations that promote mitogen-activated protein kinase (MAPK) signaling. MEK inhibitors are approved for use in BRAF-mutated melanoma; however, early-phase clinical trials show occasional responses in driver-negative melanoma, suggesting other alterations conferring MAPK/ERK dependency. To identify additional structural alterations in melanoma we evaluated RNA-Seq from a set of known MAPK/ERK regulators using a novel population-based algorithm in The Cancer Genome Atlas (TCGA). We identified recurrent MAP3K8 rearrangements in 1.7% of melanomas in TCGA, occurring in over 15% of tumors without known driver mutations (BRAF, NRAS, KIT, GNAQ, GNA11 and NF1). Using an independent tumor set we validated a similar rearrangement frequency by fluorescence in situ hybridization. MAP3K8-rearranged melanomas exhibit a low mutational burden and absence of typical UV-mutational patterns. We identified two melanoma cell lines that harbor endogenous truncating MAP3K8 rearrangements that demonstrate exquisite dependency. Rearrangement and amplification of the MAP3K8 locus in melanoma cells results in increased levels of a truncated, active MAP3K8 protein; oncogenic dependency on the aberrant MAP3K8; and, a concomitant resistance to BRAF inhibition and sensitivity to MEK or ERK1/2

[*]**Corresponding author:** Brian Lehmann, Vanderbilt-Ingram Cancer Center, 652 Preston Research Building, Nashville, TN 37232, USA. Phone: 615-936-1512; Fax: 615-936-2294, brian.d.lehmann@vanderbilt.edu.

Authors' contributions

Conception and design: B.D. Lehmann and J.A. Pietenpol

Development of methodology: B.D. Lehmann, T. M. Shaver and J.A. Pietenpol

Acquisition of data (provided tissue, acquired and managed patients, provided facilities, etc.): D.B. Johnson, Z. Li and P.I. Gonzalez Ericsson

Analysis and interpretation of data (e.g., statistical analysis, biostatistics, computational analysis): B.D. Lehmann, T. M Shaver, P.I. Gonzalez Ericsson, Y. Shyr, M.A. Sanders and J.A. Pietenpol

Writing, review, and/or revision of the manuscript B.D. Lehmann, T.M. Shaver and J.A. Pietenpol

Administrative, technical, or material support (i.e., reporting or organizing data, constructing databases): V. Sanchez, Y. Shyr and B.D. Lehmann

Study supervision: B.D. Lehmann and J.A. Pietenpol

Conflict of interest: The authors declare no potential conflicts of interest.

Disclosure of Potential Conflicts of Interest

The authors have no potential conflicts of interest to disclose.

inhibition. Our findings reveal and biochemically characterize targetable oncogenic MAP3K8 truncating rearrangements in driver mutation-negative melanoma; and provide insight to therapeutic approaches for patients with these tumors. These data provide rationale for using MEK or ERK inhibitors in a subset of driver-negative, MAPK/ERK-dependent melanomas harboring truncating MAP3K8 rearrangements.

Implications: This is the first mechanistic study and therapeutic implications of truncating MAP3K8 rearrangements in driver-negative melanoma.

Introduction

Recent advances in sequencing technology and the efforts of The Cancer Genome Atlas (TCGA) have led to the genomic characterization of many cancers[1]. In melanoma, recurrent “driver” mutations have been identified in BRAF, NRAS, KIT, NF1, GNAQ, and GNA11; these clinically actionable alterations now define molecular subsets of the disease that oncologists use to properly align patients with effective targeted therapy[2–4]. BRAF V600 mutations occur in nearly 50% of melanomas and are predictive for sensitivity to RAF inhibitors, whereas activating KIT and NRAS mutations may predict response to receptor tyrosine kinase and MEK inhibitors, respectively. However, 10–20% of melanomas lack recurrent driver mutations and thus have no effective targeted therapy options. Clinically, there is evidence of MAPK dependency in the absence of known driver alterations from a phase I trial in which four of 20 patients with wild-type BRAF and NRAS responded to MEK inhibition[5]. These findings suggest that additional alterations may activate the MAPK/ERK pathway in melanomas lacking currently catalogued driver mutations. We recently identified BRAF kinase gene fusions occurring exclusively in driver-negative melanomas, further emphasizing the dependency of melanomas on MAPK signaling[6]. Using a focused approach for known MAPK regulators, we examined RNA-Seq data from TCGA for evidence of structural gene alterations and identified recurrent MAP3K8 rearrangements in six melanoma tumors (1.7% overall). The rearrangements were exclusive to driver-negative melanomas (6 of 38, 15.8%) and result in a truncated, active MAP3K8.

Materials and Methods

TCGA Analysis

RNA-Seq gene expression data for TCGA skin cutaneous melanoma (SKCM) study were obtained from the Broad GDAC Firehose (http://gdac.broadinstitute.org/). Exon-level RSEM mRNA expression (stddata_2016_01_28 run) was downloaded and plots generated in sequential exon order based on RefGene (hg19) annotation. Tumors with highly discordant expression between exons 7 and 8 of MAP3K8 were further inspected for evidence of hybrid sequences by examining aligned RNA-Seq files downloaded from the Cancer Genomics Hub. The number of discordant read pairs and breakpoint-spanning reads were determined for each of the suspected tumors. For tumors with matching whole-genome DNA-Seq, files were downloaded and inspected for breakpoint-spanning reads. Additional DNA validation was obtained from copy number evaluation using IGV displaying genome wide copy number (SNP6) data (Broad Firehose stddata_2016_01_28). Mutation annotation files (.maf) for SKCM were downloaded from GDAC Firehose (stddata_2016_01_28 run) and the total

number of variants per sample determined. To determine the UV induced mutations, the C>T and G>A mutations were extracted and the mutation frequency calculated for each sample.

Melanoma cell line copy number analysis—Normalized array-based Comparative Genomic Hybridization (CGH) of 33 melanoma cell lines were downloaded (GSE38946) and annotated with Agilent SurePrint G3 Human CGH Microarray platform (GPL9777). MAP3K8 log10 Cy5/Cy3 copy number ratios were evaluated across the dataset.

Discordant MAP3K8 transcript expression from gene expression microarray—Gene expression for cancer cell lines obtained from the Cancer Cell Line Encyclopedia (CCLE_Expression_2012–09–29.res., https://portals.broadinstitute.org/ccle/data/) and melanoma cell lines (GSE7127). Expression values from probes hybridizing to intron 1 (235421_at) or the 3'UTR (205027_s_at) of MAP3K8 were extracted and expression discordance evaluated by scatterplot and expression ratios.

Cell culture—WM3311 cells (Rockland, Limerick, PA, purchased May 2016) were maintained in 1:5 Leibovitz's L-15/MCDB15 media supplemented with 1.68mM $CaCl_2$ and 2% fetal bovine serum (FBS). SK-MEL-28 cells (ATCC, March 2010, provided by Dr. Ann Richmond Vanderbilt University, authenticated by short tandem repeat profiling, November 2013) were cultured in F12 (Gibco 61870) supplemented with 5% (v/v) FBS (Gemini) and maintained in 100 U/mL penicillin and 100 μg/mL streptomycin (Gemini). D35 cells (provided by Dr. Nick Hayward, QIMR Berghofer Medical Research Institute, March 2016) were grown in RPMI media supplemented with 5% (v/v) FBS. Cells were used within one to two months after thawing and tested negative for mycoplasma contamination (MycoAlert, Lonza) prior to cryopreservation and upon thawing. WM3311 and D35 cells were not authenticated as they were directly obtained from source and RNA-seq data lacked driver mutations, consistent with original mutational characterization.

Expression Vectors

Sequence encoding the HA tag was added to the N-terminus of cDNA encoding full-length MAP3K8 in a pDONOR322 vector (#23538, Addgene) by PCR. Site-directed mutagenesis was performed on full-length MAP3K8 to generate a stop codon (aa 425). Isoleucine (ATT) was added by site-directed mutagenesis prior to the stop codon of MAP3K8–425-stop vector to generate coding sequence identical to patient TCGA-ER-A196. Catalytically inactive kinase versions of full-length and MAP3K8ΔC were generated by site-directed mutagenesis (K167R) as previously demonstrated[7]. A table of all primers used is available in Supplemental Table 1. All plasmids were subcloned into the retroviral vector pCLXSN (#12343, Addgene) with Gateway cloning L/R reactions and colonies were sequence verified. Stably transfected cell lines were generated using retroviruses packaged from Phoenix cells (Orbigen) and selected with 0.3 mg/mL geneticin (Sigma).

Immunobloting

SK-MEL-28 cells were lysed in 60 mm plates 3 h after treatment with increasing doses of inhibitors (vemurafenib, trametinib or SCH772984) in media containing 0.5% FBS. All cells

were lysed in RIPA buffer supplemented with protease and phosphatase inhibitors. Cell lysates (40 μg) were separated on polyacrylamide gels and transferred to polyvinyl difluoride membranes (Millipore). Immunoblotting was performed using HA 6E2 (1:1000, Cell Signaling #2367S), MEK (1:500, Cell Signaling #4694S), phospho-MEK1/2 Ser17/Thr221 (1:500, Cell Signaling #9121S), GAPDH (1:1000, Millipore, MAB374), phospho-Erk1/2 Thr202/204 (1:1000, Cell Signaling, #4370), total Erk1/2 (1:1000, Cell Signaling, #9107) and MAP3K8 (R&D Systems, MAB4586). Protein half-life determined from double-log transformation immunoblot quantification (ImageJ) following cyclohexamide (100μg/mL) treatment.

Immunofluorescence

SK-MEL-28 cells stably expressing MAP3K8 were fixed, permeabilized and blocked with 10% goat serum/PBS. Cells were then incubated with primary mouse anti-HA antibody (Cell Signaling #2367) and secondary goat anti-mouse AlexaFuor-94 (Thermofisher) and counterstained with DAPI (0.5 μg/mL) prior to microscopy.

Drugs and viability assays

SK-MEL-28, WM3311 and D35 cells were seeded in triplicate (750 cells/well) in 96-well plates. After overnight attachment, growth medium was replaced with either medium (control) or medium containing half-log serial dilutions of vemurafenib (Selleckchem), MEK inhibitor trametinib (Selleckchem) or SCH772984 (Selleckchem). Viability was assessed at 72 h by incubating cells with alamarBlue (Invitrogen), per manufacturer's protocol. Half-maximal inhibitory concentration (IC_{50}) values were determined as previously described[8].

siRNA knockdown

WM3311 and D35 cells (5000 cells/well) were reverse-transfected with 0.2 μL/well RNAimax lipid (Invitrogen) and 25nM of non-targeting control (Qiagen), cell death control (Qiagen) or four siRNAs targeting MAP3K8 (D-003511–07, D-003511–08, D-003511–09, D-003511–10, Dharmacon/GE Life Sciences) siRNA in 96-well culture dishes. Viability was measured by alamarBlue after 72 h and mean and standard deviation determined from 24 technical replicates. After viability measurement, cells were harvested and lysates were generated with RIPA buffer for immunoblot analysis.

Positional imbalance qPCR—Quantitative reverse transcription-PCR (RT-PCR) were performed as described previously(9,12,19). Two primers were designed (primer3) to exon regions or exonic junctions both upstream and downstream of intron 7 of MAP3K8. Primer sequences can be found in Supplemental table 1. Gene expression measurements were normalized relative to GAPDH.

RNA sequencing

RNA was isolated from WM3311 and D35 cells using the Aurum Total RNA Mini kit (Bio-Rad). RNA was submitted to the Vanderbilt Technologies for Advanced Genomics core for library preparation and RNA-seq. Paired-end sequencing performed on Illumina Hi-seq at a

depth of 98 million reads (see supplemental methods for alignment). Raw reads were trimmed to remove adapter sequences with Flexbar v2.4 and aligned to HG19 using Mapslice 2.2.1 and UBU v1.2 according to the TCGA RNA-Seq v2 pipeline (https://cghub.ucsc.edu/docs/tcga/UNC_mRNAseq_summary.pdf, 7/31/2013 revision). Reference data and custom scripts for exon-level expression quantification were downloaded from the UNC database as referenced in the protocol. Raw sequencing data have been deposited at the NCBI Sequence Read Archive under accession numbers SRX5765980 and SRX5765981.

Break-apart fluorescence in situ hybridization

For fluorescence in situ hybridization (FISH) analysis, tissue sections were hybridized overnight with the probes (Empire Genomics): RPCI-11#257J14 (Orange, 5-TAMRA-dUTP) and RPCI-11#122B23 (Green, 5-Fluorescein-dUTP). See supplemental methods for detailed methods and scoring. Briefly, deparaffinization, protease treatment and washes were performed. After pretreatment, slides were denatured in the presence of 10 μl of the probe for 6 min at 72°C and hybridized at 37°C overnight in StatSpin (Thermobrite, Abbott Molecular, Inc.). Post-hybridization saline sodium citrate (SSC) washes were performed at 72°C and slides were stained with DAPI before analysis. Representative images of tumor cells were captured using Cytovision software and positive cells quantified.

Tumor tissue was scanned at 40x for evidence of chromosomal rearrangement (break apart) and subsequent increased copy number/amplification of upstream MAP3K8 using a fluorescent microscope (Olympus BX60). Images for cell counting were captured using a 100x objective using Cytovision software. Ten to forty tumor cells per case were scored by two independent pathologists (PIGE and MS). Cells with two yellow signals were considered to lack evidence of MAP3K8 rearrangement. Cells with red (MAP3K8 upstream probe) and green (MAP3K8 downstream probe) signals demonstrated chromosomal break apart. Cells with multiple red signals are consistent with amplification of the upstream portion of MAP3K8. Only cells with red and green signals, red and yellow signals or yellow, red and green signals were evaluated. The ratio of red to green signals and the average MAP3K8 upstream (red) copy number per cell were calculated.

Statistical Analysis

Kaplan-Meier and log-rank tests were used to estimate and compare survival curves. Fisher's exact t-test used to determine significance of single categorical variable and Chi-squared used for comparisons involving two categorical variables.

Results

Identification of truncating MAP3K8 rearrangements in driver-negative melanoma

To identify structural alterations in MAPK/ERK pathway genes, we performed a targeted evaluation of skin cutaneous melanoma (SKCM) transcript expression from TCGA. Exon-level RNA-Seq expression was analyzed using Segmental Transcript Analysis as previously described[9], and samples with highly discordant expression across the length of the gene were investigated further. We identified six tumors that exhibited high MAP3K8 transcript levels across exons one to seven and low expression of exon eight and the 3'UTR (Fig. 1A).

Despite low-level expression of the 3' region of the normal gene, these truncated transcripts displayed the highest levels of MAP3K8 expression in the TCGA cohort (Fig. 1B and C). To determine if this decreased 3' expression was caused by a structural genomic alteration, we examined raw RNA-Seq reads in the junction between exons seven and eight and whole-genome DNA-Seq reads in the intervening intron. All six tumors displayed evidence of both discordant read pairs and breakpoint-spanning reads beginning at the end of exon seven of *MAP3K8* and ending at different inter- and intra-chromosomal positions (Table 1). We additionally found DNA-level evidence of a rearrangement within the intron between exons seven and eight in one tumor for which whole-genome sequencing was available (TCGA-ER-A196) (Fig. 1D). Whole-genome copy number analysis demonstrated abrupt changes within the same intronic region for three of the five remaining samples, providing additional DNA-level rearrangement evidence (Supplemental Fig. 1). While all breakpoints occurred after exon 7 of *MAP3K8*, the 3' partner was not conserved, occurring in intergenic, intronic and coding regions across multiple chromosomes (Table 1). The truncated MAP3K8 transcripts encode a protein retaining the full kinase domain but lacking the PEST protein degradation domain commonly contained in proteins with extremely short half-lives[10] (Fig. 1E). The loss of the degradation domain and negative-regulatory 3' UTR likely selects for this rearrangement during tumorigenesis. In the six TCGA cases, the additional amino acids encoded by the 3' partners lack sequence consensus and add only 2–44 amino acids before terminating at a stop codon (Supplemental Fig. 2).

Of the 343 tumor samples evaluated, 305 (88.9%) had mutations in known driver genes (BRAF, NRAS, NF1, KIT, GNAQ and GNA11), with 38 samples lacking driver mutations (Supplemental Table 2). C-terminal truncating MAP3K8 rearrangements (MAP3K8ΔC) occurred in six of 343 total melanomas (1.7%), but all were exclusively observed in driver-negative melanomas (6 of 38, 15.8%), representing a highly significant enrichment (p=1.275e-06) (Fig. 1F).

Cutaneous melanomas typically exhibit elevated mutation rates compared to other tumors, with a high frequency of cytosine to thymine (C > T) transitions generated from misrepair of UV-induced pyrimidine dimers[11]. Tumors with MAP3K8 alterations had significantly fewer mutations in coding regions compared with other melanomas (average 53 vs. 857 mutations/tumor, p=1.66e-16; Fig. 1G). The frequency of UV-associated mutations (C>T and G>A) was also significantly lower in MAP3K8-rearranged samples (40% vs. 74%, p=0.0023) and together with the decreased mutational burden, suggest that these tumors are likely not associated with sun exposure (Fig. 1H).

Patients with MAP3K8 rearrangements were clinically similar to melanoma as a whole, displaying similar distribution between males and females, primary and metastatic disease, and across ages (Fig. 1I and Supplemental Table 2). Overall survival was significantly reduced for patients harboring MAP3K8 rearrangements compared to all other melanomas (median survival 20.5 vs. 80.6 months, p=0.0046), however given the small sample size (n=6) these data should be interpreted with caution and require further validation, as differing treatments could have also impacted the interpretation of these results (Supplemental Fig 1).

MAP3K8 gene rearrangements generate truncated proteins activate MEK and ERK1/2 and confer cell sensitivity to MEK and ERK inhibition

To determine the functional and potential therapeutic significance of MAP3K8 truncating rearrangements, we generated HA-tagged cDNAs encoding full-length MAP3K8 and a chimeric transcript encoding a truncated MAP3K8 (MAP3K8ΔC) that was identified in a TCGA melanoma specimen (TCGA-ER-A196) and validated by DNA-Seq. HA-tagged full-length MAP3K8, MAP3K8ΔC, kinase-inactive (KI) versions of both, and an empty vector control were ectopically expressed in BRAF wild-type 293T cells. MAP3K8 expression resulted in detection of a single 53 kD or 49 kD protein band for full-length and truncated MAP3K8, respectively; these Western signals represent the long (aa 1–467) isoform, as the shorter isoform generated from an alternative start codon (aa 30–467) is not detectable by the addition of an N-terminal HA tag (Fig. 2A)[12]. Over expression of full-length and to a greater degree truncated MAP3K8 increased both phosphorylated forms of MEK1/2 and ERK1/2 (Fig. 2A).

To define the functional role of MAP3K8 truncations in melanoma cells, we generated stable cell lines expressing exogenous HA-tagged MAP3K8 using SK-MEL-28 cells, a well-characterized melanoma cell line harboring a BRAF V600E mutation that is sensitive to BRAF and MEK inhibitors[12]. MAP3K8 protein localization was not altered by truncation or kinase inactivation, with all forms diffusely localized throughout the cytoplasm (Fig. 2B) similarly to previous reports[13]. MAPK pathway activation and response to inhibition (Fig. 2C) were evaluated in cells expressing each MAP3K8 variant. At baseline, expression of full-length and truncated MAP3K8 did not alter phosho-ERK1/2 levels; however, both displayed elevated phospho-MEK levels dependent on MAP3K8 kinase activity (Fig. 2D, F and H, lanes 1, 5 and 9). Dose-dependent reductions in phospho-MEK and phospho-ERK1/2 were observed after treatment with the RAF inhibitor vemurafenib in the engineered SK-MEL-28 cells expressing the empty vector control or kinase inactive MAP3K8 proteins (Fig. 2D). However, expression of MAP3K8ΔC and to a lesser extent full-length MAP3K8 activated MAPK signaling (p-MEK and p-ERK1/2) in the presence of vemurafenib, demonstrating that MAP3K8 activates ERK signaling downstream of BRAF (Fig. 2D; lanes 6–8). To determine if sustained ERK signaling from MAP3K8 and MAP3K8ΔC can confer resistance to BRAF inhibition, we analyzed cell viability after treatment of the panel of SK-MEL-28 cells with vemurafenib. Cells expressing the empty vector control and kinase-inactive MAP3K8 proteins displayed similar sensitivity to vemurafenib, while cells expressing either full-length MAP3K8 or MAP3K8ΔC were significantly less sensitive to BRAF inhibition (Fig. 2E). The half-maximal inhibitory concentration (IC_{50}) was significantly higher for both kinase-active forms (p=0.0005) (Supplemental Fig. 3).

To determine if MAP3K8 activates the MAPK pathway downstream of BRAF, we treated cells with increasing doses of MEK (trametinib) and ERK (SCH772984) inhibitors. MAP3K8ΔC and to a lesser extent full-length MAP3K8 sustained p-MEK levels in the presence of MEK and ERK inhibition (Fig. 2F and H). However, both inhibitors decreased p-ERK1/2 in cells expressing all of the MAP3K8 variants (Fig. 2F and H). Inhibition of ERK with SCH72984 was confirmed by decreased phosphorylation of the substrate RSK1 (Fig. 2H). The uniformly decreased p-ERK levels were paralleled by similar sensitivities to

trametinib and SCH772984 among all engineered SK-MEL-28 cells, demonstrating that MAP3K8 activates MAPK upstream of ERK and MEK, and that tumors with MAP3K8ΔC rearrangements may retain sensitivity to MEK and ERK but not BRAF inhibition (Fig. 2G and I).

Since MAP3K8ΔC rearrangements result in a 44 amino acid truncation, including part of the PEST protein degradation domain, we evaluated the protein half-life of full-length and truncated MAP3K8 protein expressed in 293T cells by immunoblot at serial time points after cyclohexamide treatment (Fig. 2J). While MAP3K8 and MAP3K8ΔC were expressed at similar levels at baseline, MAP3K8ΔC displayed an extended half-life compared to MAP3K8 when analyzed with HA (4.8 vs. 1.5 h) or MAP3K8 (9.3 vs. 2.2 h), antibodies, demonstrating that PEST domain loss increases the stability of the truncated protein (Fig. 2K and L).

Melanoma cell lines harboring endogenous MAP3K8 rearrangements are dependent on MAP3K8 and sensitive to MEK and ERK inhibition—To identify cell line models that may harbor endogenous MAP3K8 truncations we examined MAP3K8 DNA copy number from array comparative genomic hybridization (CGH) performed on 33 melanoma cell lines (GSE38946). Within this dataset we identified one cell line, WM3311, with a focal MAP3K8 DNA amplification (Fig. 3A). Detailed examination suggested a chromosomal breakpoint with five of six probes located in introns (1, 3 and 6) and exons (3 and 4) displaying copy increases, while the sixth probe corresponding to the 3’ UTR appearing copy-neutral (Fig. 3B). Using RNA isolated from WM3311, we performed qRT-PCR for amplicons upstream and downstream of the potential breakpoint within MAP3K8 to determine the impact of the abrupt copy number change on transcript levels. MAP3K8 expression was 1347-fold greater upstream of the breakpoint (relative expression 0.1759 vs. 0.0005), strongly suggesting that the WM3311 cell line harbors an endogenous rearrangement transcribing a truncated MAP3K8 transcript (Fig. 3C).

Given the DNA copy number and RNA positional qPCR imbalance evidence for a MAP3K8 rearrangement in WM3311 cells, we performed RNA-seq. Reads mapping to MAP3K8 exons verified low levels of expression in exon 8 and 3’ UTR (TPM= 0.53), with 1472-fold more transcript upstream of the breakpoint (average TPM exons 1–7 = 784) (Fig. 3D). RNA-Seq provided definitive evidence (426 discordant read pairs and 101 breakpoint-spanning reads) for an intrachromosomal MAP3K8 rearrangement (chr10:30748430-chr10:32808416) generating a hybrid transcript between exon 7 of MAP3K8 and the strand antisense to intron 12 of CCDC7; the resulting transcript would encode a truncated MAP3K8 protein with an additional 50 amino acids (Fig. 3E). The WM3311 cell line is one of seven from a collection of 93 melanoma cell lines generated by the Wistar Institute that do not contain mutated BRAF, NRAS, KIT or GNAQ genes (Supplemental Table 3), providing supporting evidence for the driver mutation-negative rearrangement pattern seen in TCGA.

To determine if WM3311 cells demonstrate oncogenic dependence on endogenous truncated MAP3K8, we performed siRNA MAP3K8 knockdown with four individual siRNAs. Both the canonical (aa 1–424) and alternate start site (aa 30–424) forms of MAP3K8 decreased with siRNA knockdown (Fig. 3F); variable knockdown efficiency between the individual

siRNAs correlated with reductions in phosphorylated and total MEK and ERK1/2 (Fig. 3F). MAP3K8 siRNA-treated cells exhibited significantly decreased viability (26–57% relative to nontargeting control) that correlated with degree of knockdown (Fig. 3G). Colony-forming ability of WM3311 cells was determined after MAP3K8 siRNA knockdown. All four MAP3K8 siRNAs decreased colony number and size, with the two most effective siRNAs decreasing colony formation to an extent similar to the cell death control (Fig. 3H).

To determine if pharmaceutical agents are effective in targeting cells dependent on truncated MAP3K8, we treated WM3311 cells with several inhibitors of the MAPK/ERK pathway (Fig. 3I). Similar to SK-MEL-28 cells with exogenous MAP3K8ΔC overexpression, WM3311 cells were insensitive to vemurafenib, failing to achieve an IC_{50} at a 3μM dose (Fig. 3I). However, WM3311 cells were extremely sensitive to MEK (trametinib IC_{50}=419+/−79pM) and partially sensitive to ERK1/2 (SCH772984 IC_{50}=123+/−32nM) inhibition, demonstrating dependency on ERK downstream of RAF (Fig. 3I). In contrast to trametinib and SCH772984, vemurafenib treatment produced no change in phospho-ERK1/2 levels (Fig. 3J).

To identify additional cell lines harboring endogenous MAP3K8 rearrangements, we evaluated additional microarray expression datasets for discordances in MAP3K8 transcript expression proximal and distal to the breakpoint similar to those patients identified in the TCGA dataset (Supplemental Fig. 4Aand B). We examined MAP3K8 RNA expression using probes to intron 1 and the 3’ UTR of MAP3K8 from microarray data performed on 1036 cell lines in the cancer cell line encyclopedia (CCLE). Within this dataset there was a near perfect correlation between expression in intron 1 and the 3’ UTR (Supplemental Fig. 4Cand D)[14], suggesting that these probes were specific to MAP3K8 expression. We applied a similar analysis to a melanoma cell line dataset (GSE7127) and identified four cell lines out of 63 (6.3%) with discordant MAP3K8 expression (Fig. 4A). We selected the cell line with the highest intron 1 to 3’ UTR expression ratio (D35) for further evaluation (Fig. 4B). We performed similar position PCR upstream and downstream of the potential breakpoint. Unlike the MAP3K8 rearrangement-negative melanoma cell line SK-MEL-5 (Fig. 4C), D35 cells displayed high 5’ MAP3K8 expression levels that were substantially diminished after the exon 7/8 junction (Fig. 4D), similar to the expression pattern of WM3311 cells and confirming the discordant expression with microarray probes (Fig. 4A).

We performed RNA-Seq on D35 cells and demonstrate the diminished expression in the last exon (Fig. 4E). Further analysis identified definitive evidence (30 discordant read pairs and 30 breakpoint-spanning reads) for an interchromosomal *MAP3K8* rearrangement (chr10:30748415-chr6:10543467) generating a hybrid transcript between exon 7 of *MAP3K8* and the intronic region (I3–I4) of *GCNT2* (Fig. 4F). D35 cells are wild-type for BRAF and NRAS, consistent with the status of these genes in MAP3K8-rearranged patient tumors. D35 cells were dependent on MAP3K8 as knockdown diminished viability and colony forming of D35 cells (Fig. 4G). To determine the sensitivity of D35 to MAPK/ERK pathway inhibitors we treated cells with increasing doses of vemurafenib, trametinib and SCH772984. D35 cells were sensitive to MEK and ERK1/2 inhibition, but were resistant to BRAF inhibition (Fig. 4H), similar to WM3311 cells harboring an endogenous MAP3K8 rearrangement (Fig. 3I) and SK-MEL28 cells overexpressing truncated MAP3K8 (Figs. 2E,

G and I). Immunoblot analysis of MAPK/ERK pathway supported the viability data, with trametinib and SCH772984 decreasing and vemurafenib not effecting p-ERK levels (Fig. 4H). To determine if MAP3K8 dependency was specific to cells harboring the rearrangement (WM3311 and D35) we treated a panel of five additional melanoma cell lines lacking the rearrangement with siRNAs targeting MAP3K8. Viability was was not significantly affected in melanoma cell lines lacking the rearrangement and only cell lines harboring truncated MAP3K8 (WM3311 and D35) were sensitive to siRNAs targeting MAP3K8 (Supplemental Fig. 5).

To identify additional potential pathways that could be targeted, we performed differential gene expression and pathway analysis of RNA-seq from MAP3K8- truncated compared with all other melanomas (Supplemental Fig. 6). Tumors with truncated MAP3K8 were significantly enriched genes in pathways relating to the unfolded protein response, MYC targets, E2F targets and G2M checkpoint. However, MAP3K8 tumors were significantly depleted in pathways involved in the immune system, immunoreguatory interactions, adaptive immune system and cytokine receptors pathway gene expression, suggesting an immune-depleted microenvironment that may not be amenable to immune checkpoint therapy.

Break-apart fluorescence in situ hybridization identifies MAP3K8 rearrangements in an independent tumor dataset—To demonstrate a clinically relevant strategy beyond sequencing to identify potential future patients harboring the rearrangement, we devised a break-apart fluorescence *in situ* hybridization (FISH) approach using fluorescently labeled DNA probes flanking the breakpoint (Fig. 5A). Normal lymphocyte tissue exhibited a pair of yellow signals in each cell, indicating two copies of intact wild-type MAP3K8 (Fig. 5B). WM3311 cells harboring a known rearrangement displayed a single yellow signal with several individual red signals, indicating a breakpoint and amplification of MAP3K8 proximal to the breakpoint, consistent with CGH data (Fig. 5C). D35 cells displayed split green and red signals indicting a single breakpoint without amplification and validating the discordant mRNA expression and truncated MAP3K8 protein (Fig. 5D). To determine if MAP3K8 rearrangements could be identified in an independent collection of melanomas, we performed break-apart FISH on a tissue microarray generated from 14 BRAF-mutated, 15 NRAS-mutated, and 39 wild-type melanomas from Vanderbilt University Medical Center (Supplemental Table 4). We identified seven tumors positive for MAP3K8 rearrangements by FISH, with either individual split green and red signals (Fig. 5E), a single (Fig. 5F) or double (Fig. 5G) yellow signal with multiple red signals indicating amplification of MAP3K8 prior to the breakpoint in a manner similar to the rearrangement-positive WM3311 cells (Fig. 5E–G). All seven breakpoint-positive specimens were identified in tumors lacking BRAF or NRAS mutations (Supplemental Fig. 7).

Discussion

Although MAP3K8 function has largely been evaluated in macrophages, where it is required for lipopolysaccharide-mediated MAPK/ERK pathway activation[13,15], several older studies provide evidence of MAP3K8 proto-oncogenic activity. The oncogenic potential of

MAP3K8 was first described over two decades ago when DNA derived from a human thyroid carcinoma cell line (TCO4) demonstrated the ability to transform hamster SHOK cells, thus identifying a new transforming gene termed *cot* (cancer Osaka thyroid)[16]. Additionally, a murine viral insertional screen identified a common viral integration site in MAP3K8, termed tumor progression locus 2 (Tpl-2), that was associated with the formation of T-cell lymphomas[17]. Integration repeatedly occurred in the intron between exons seven and eight of MAP3K8, leading to a truncated transcript ending in the proviral long terminal repeat. Importantly, the N-terminal truncated portion of the gene was shown to rapidly induce T-cell lymphoblastic lymphomas when expressed under a T cell-specific promoter in transgenic mice[7]. However, to date, with the exception of rare activating MAP3K8 mutations in lung cancer[18], MAP3K8 alterations have largely been undescribed in human cancers.

With this study, we offer the first description and biochemical characterization of oncogenic MAP3K8 alterations in human cancer, occurring exclusively in driver mutation-negative melanoma. We identified six carboxy-terminal truncating MAP3K8 rearrangements in both primary and metastatic melanomas that were associated with decreased overall survival.

All the truncating rearrangements in MAP3K8 occur in the intronic region, separating both the stabilizing PEST protein domain in exon 8 and the 3’ UTR from the kinase domain. This event likely upregulates MAP3K8 on two levels with the loss of the 3’ UTR causing upregulation of truncated transcript and loss of the PEST protein domain causing increased stability of the truncated protein, leading to increased activity.

Using a break-apart FISH strategy, we identified seven additional MAP3K8 rearrangements in an independent collection of human melanomas; as observed in the TCGA tumors, these rearrangements were found exclusively in driver mutation-negative melanomas with a similar frequency (17.9% vs. 15.8%). The break-apart FISH strategy and sequencing-based approaches have the potential to identify patients with MAP3K8 truncating rearrangements.

At this time, no effective targeted therapy options are available for these driver mutation-negative patients. Furthermore, while immune checkpoint inhibitors cause durable responses in many melanoma patients, clinical benefit has been strongly associated with tumors displaying higher mutation burdens[19,20]. Importantly, melanomas with MAP3K8 rearrangements have on average 16-fold fewer nonsynonymous mutations than melanoma as a whole. MAP3K8 rearranged melanomas also lack the hallmark UV mutation pattern (C>T and G>A) caused by misrepair of thymidine dimers from UV exposure. Of note, one of the MAP3K8 rearrangements occurred in the rare acral lentiginous histological subtype typically observed in areas with low UV-exposure such as palms, soles, and nail beds. These findings are consistent with a previous publication in which triple wild-type (BRAF, NRAS and NF1) status was associated with a lower rate of UV-associated mutations[4]. Therefore, immune checkpoint therapy combinations are unlikely to benefit patients with melanomas carrying MAP3K8 truncations. This is supported by a recent publication in which a patient rapidly progressed on first line ipilimumab and pembrolizumab therapy, and then progressed after receiving the oncolytic vaccine talimogene laherparepvec (TVEC) prior to achieving responses to trametinib and ERK inhibition. Cell lines with MAP3K8 truncations displayed

sensitivity to both MEK and ERK inhibitors, providing rationale for a dual combination approach.

Both MAP3K8 and MAP3K8ΔC expression caused and increased phosphorylated MEK and resistance to vemurafenib in a BRAF-mutated cell line, validating a recent kinome screen in which full-length MAP3K8 expression conferred vemurafenib resistance in BRAF mutated cells[12]. In this previous study, the authors also identified one BRAF-mutated melanoma cell line that was MAP3K8-amplified and clinical evidence for increased MAP3K8 transcript in post-treatment clinical specimens from patients not responding to vemurafenib[12]. While the data clearly implicate MAP3K8 in BRAF-mutant resistant disease, we were unable to identify MAP3K8 rearrangements in BRAF inhibitor-resistant disease form 19 patients [21] and seven patients from another study [22]. Truncating MAP3K8 rearrangements appear to be unique to primary melanoma tumors lacking known drivers, while MAP3K8 amplification occurs as a mechanism of resistance to RAF inhibitors in treatment-resistant disease.

Using additional MAPK/ERK pathway inhibitors, we demonstrated that cells expressing MAP3K8ΔC exhibit activated MEK and retain sensitivity to MEK and ERK inhibitors. There is already precedence for MEK inhibitor activity in BRAF wild-type patients (10% response rate) with trametinib and unidentified MAP3K8 rearrangements may have contributed to these responses[5]. Using a variety of genomic approaches, we identified endogenous MAP3K8 rearrangements in two cell lines lacking known driver mutations that displayed exquisite dependency on MAP3K8 and sensitivity to MEK inhibition. A recent study has identified truncating MAP3K8 alterations in a spitzoid melanoma lacking known driver mutations responding to the ERK in inhibitor LTT462 in a clinical trial, validating the preclinical sensitivity of cell lines with truncating MAP3K8 alterations to MEK and ERK inhibitors in the current study [23]. These truncating MAP3K8 rearrangements highlight the diverse mechanisms of MAPK/ERK pathway activation in melanomas and provide a tractable biomarker to identify additional patients that may benefit from targeted inhibition of MEK and ERK.

Supplementary Material

Refer to Web version on PubMed Central for supplementary material.

Acknowledgments

The results published here are in part based upon data generated by TCGA Research Network: http://cancergenome.nih.gov. We kindly thank Nick Hayward for supplying the D35 cell line. **Acknowledgements of research of research support:** B.D.L. was supported by Komen CCR13262005. T.M.S. was supported by CA183531, GM008554, and HHMI MIG56006779. D.B.J. was supported by K23CA204726. J.A.P. was supported by CA098131 and Komen SAC110030.

Abbreviations:

CGH	comparative genomic hybridization
cot	cancer Osaka thyroid

FISH	fluorescence in situ hybridization
IC_{50}	half-maximal inhibitory concentration
MAPK	mitogen-activated protein kinase
Tpl-2	tumor progression locus 2
SKCM	skin cutaneous melanoma
TVEC	talimogene laherparepvec

References

1. Cancer Genome Atlas Research Network. Comprehensive genomic characterization defines human glioblastoma genes and core pathways. Nature. 2008;455: 1061–1068. doi:10.1038/nature07385 [PubMed: 18772890]
2. Hodis E, Watson IR, Kryukov GV, Arold ST, Imielinski M, Theurillat J-P, et al. A landscape of driver mutations in melanoma. Cell. 2012;150: 251–263. doi:10.1016/j.cell.2012.06.024 [PubMed: 22817889]
3. Cancer Genome Atlas Network. Genomic Classification of Cutaneous Melanoma. Cell. 2015;161: 1681–1696. doi:10.1016/j.cell.2015.05.044 [PubMed: 26091043]
4. Krauthammer M, Kong Y, Bacchiocchi A, Evans P, Pornputtapong N, Wu C, et al. Exome sequencing identifies recurrent mutations in NF1 and RASopathy genes in sun-exposed melanomas. Nat Genet. 2015;47: 996–1002. doi:10.1038/ng.3361 [PubMed: 26214590]
5. Falchook GS, Lewis KD, Infante JR, Gordon MS, Vogelzang NJ, DeMarini DJ, et al. Activity of the oral MEK inhibitor trametinib in patients with advanced melanoma: a phase 1 dose-escalation trial. Lancet Oncol. 2012;13: 782–789. doi:10.1016/S1470-2045(12)70269-3 [PubMed: 22805292]
6. Hutchinson KE, Lipson D, Stephens PJ, Otto G, Lehmann BD, Lyle PL, et al. BRAF fusions define a distinct molecular subset of melanomas with potential sensitivity to MEK inhibition. Clinical cancer research : an official journal of the American Association for Cancer Research. 2013;19: 6696–6702. doi:10.1158/1078-0432.CCR-13-1746
7. Ceci JD, Patriotis CP, Tsatsanis C, Makris AM, Kovatch R, Swing DA, et al. Tpl-2 is an oncogenic kinase that is activated by carboxy-terminal truncation. Genes Dev. 1997;11: 688–700. [PubMed: 9087424]
8. Lehmann BD, Bauer JA, Chen X, Sanders ME, Chakravarthy AB, Shyr Y, et al. Identification of human triple-negative breast cancer subtypes and preclinical models for selection of targeted therapies. J Clin Invest. 2011 ed. 2011;121: 2750–2767. doi:10.1172/JCI45014 [PubMed: 21633166]
9. Shaver TM, Lehmann BD, Beeler JS, Li C-I, Li Z, Jin H, et al. Diverse, Biologically Relevant, and Targetable Gene Rearrangements in Triple-Negative Breast Cancer and Other Malignancies. Cancer Res. 2016;76: 4850–4860. doi:10.1158/0008-5472.CAN-16-0058 [PubMed: 27231203]
10. Gándara ML, López P, Hernando R, Castaño JG, Alemany S. The COOH-terminal domain of wild-type Cot regulates its stability and kinase specific activity. Mol Cell Biol. 2003;23: 7377–7390. [PubMed: 14517305]
11. Pleasance ED, Cheetham RK, Stephens PJ, McBride DJ, Humphray SJ, Greenman CD, et al. A comprehensive catalogue of somatic mutations from a human cancer genome. Nature. 2010;463: 191–196. doi:10.1038/nature08658 [PubMed: 20016485]
12. Johannessen CM, Boehm JS, Kim SY, Thomas SR, Wardwell L, Johnson LA, et al. COT drives resistance to RAF inhibition through MAP kinase pathway reactivation. Nature. 2010;468: 968–972. doi:10.1038/nature09627 [PubMed: 21107320]
13. Dumitru CD, Ceci JD, Tsatsanis C, Kontoyiannis D, Stamatakis K, Lin JH, et al. TNF-alpha induction by LPS is regulated posttranscriptionally via a Tpl2/ERK-dependent pathway. Cell. 2000;103: 1071–1083. [PubMed: 11163183]

14. Barretina J, Caponigro G, Stransky N, Venkatesan K, Margolin AA, Kim S, et al. The Cancer Cell Line Encyclopedia enables predictive modelling of anticancer drug sensitivity. Nature. 2012;483: 603–607. doi:10.1038/nature11003 [PubMed: 22460905]

15. Belich MP, Salmerón A, Johnston LH, Ley SC. TPL-2 kinase regulates the proteolysis of the NF-kappaB-inhibitory protein NF-kappaB1 p105. Nature. 1999;397: 363–368. doi:10.1038/16946 [PubMed: 9950430]

16. Miyoshi J, Higashi T, Mukai H, Ohuchi T, Kakunaga T. Structure and transforming potential of the human cot oncogene encoding a putative protein kinase. Mol Cell Biol. 1991;11: 4088–4096. [PubMed: 2072910]

17. Patriotis C, Makris A, Bear SE, Tsichlis PN. Tumor progression locus 2 (Tpl-2) encodes a protein kinase involved in the progression of rodent T-cell lymphomas and in T-cell activation. Proc Natl Acad Sci USA. 1993;90: 2251–2255. [PubMed: 7681591]

18. Clark AM, Reynolds SH, Anderson M, Wiest JS. Mutational activation of the MAP3K8 protooncogene in lung cancer. Genes Chromosomes Cancer. 2004;41: 99–108. doi:10.1002/gcc.20069 [PubMed: 15287022]

19. Johnson DB, Frampton GM, Rioth MJ, Yusko E, Xu Y, Guo X, et al. Targeted Next Generation Sequencing Identifies Markers of Response to PD-1 Blockade. Cancer Immunol Res. 2016;4: 959–967. doi:10.1158/2326-6066.CIR-16-0143 [PubMed: 27671167]

20. Van Allen EM, Miao D, Schilling B, Shukla SA, Blank C, Zimmer L, et al. Genomic correlates of response to CTLA-4 blockade in metastatic melanoma. Science. 2015;350: 207–211. doi:10.1126/science.aad0095 [PubMed: 26359337]

21. Hugo W, Shi H, Sun L, Piva M, Song C, Kong X, et al. Non-genomic and Immune Evolution of Melanoma Acquiring MAPKi Resistance. Cell. 2015;162: 1271–1285. doi:10.1016/j.cell.2015.07.061 [PubMed: 26359985]

22. Kwong LN, Boland GM, Frederick DT, Helms TL, Akid AT, Miller JP, et al. Co-clinical assessment identifies patterns of BRAF inhibitor resistance in melanoma. J Clin Invest. 2015;125: 1459–1470. doi:10.1172/JCI78954 [PubMed: 25705882]

23. Newman S, Fan L, Pribnow A, Silkov A, Rice S, et al. Clinical genome sequencing uncovers potentially targetable truncations and fusions of MAP3K8 in spitzoid and other melanomas. Nat. Med 2019.

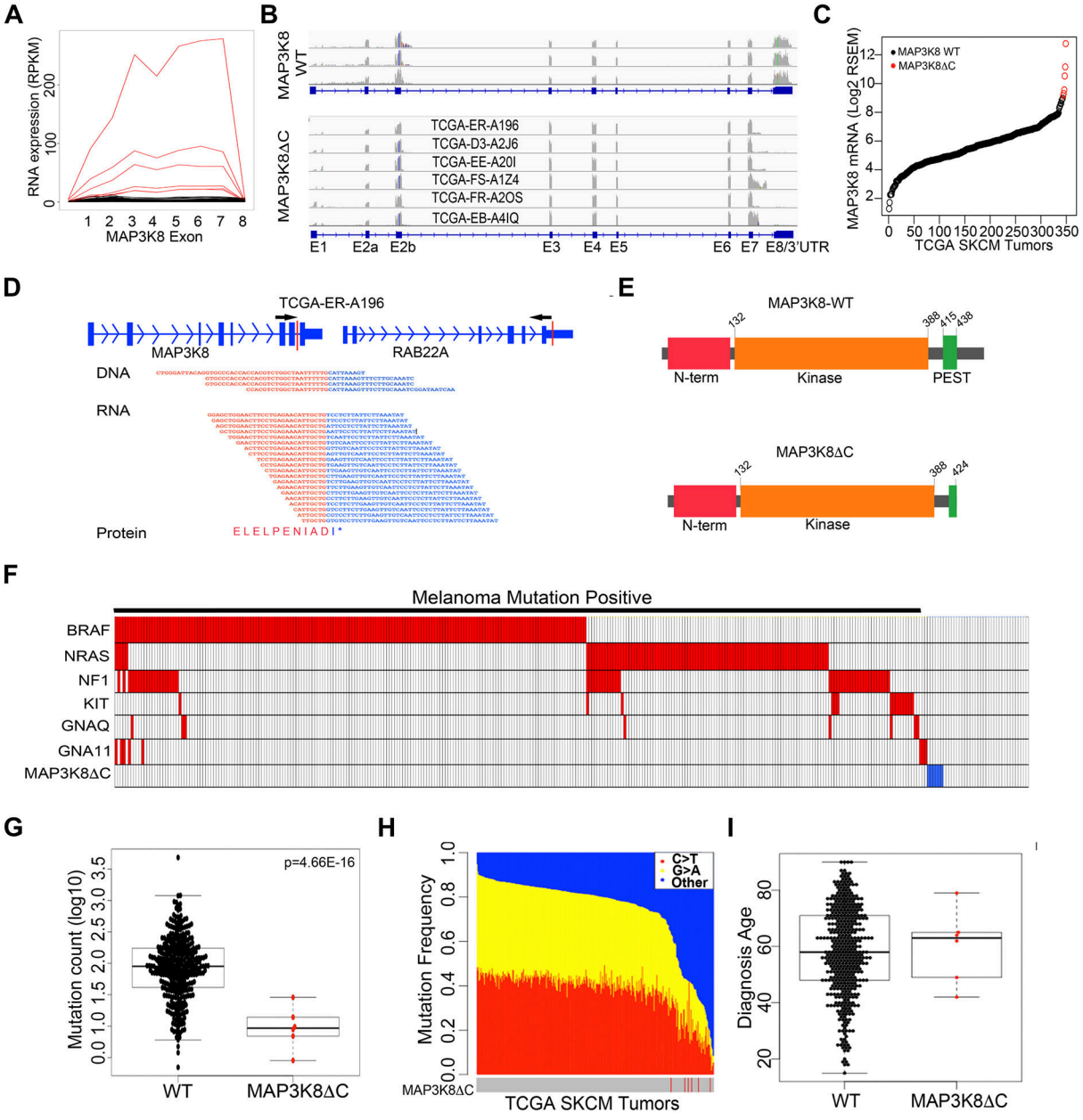

Figure 1. Identification of recurrent MAP3K8 breakpoints in melanoma.

A, Graph shows exon-level MAP3K8 mRNA expression. Samples with discordant expression indicated in red. **B**, IGV pileup tracks show normalized expression depth across MAP3K8 transcript for MAP3K8-WT tumors and six melanomas with decreased expression of exon 8 and 3'UTR. **C**, Scatterplot shows gene-level MAP3K8 mRNA expression in the TCGA melanoma cohort. **D**, Diagram of MAP3K8 and RAB22B genomic structure with breakpoints indicated by vertical red line. Breakpoint spanning reads are shown with protein translation of the hybrid transcript. **E**, Protein schematic of wild-type and truncated MAP3K8 (MAP3K8ΔC) with indicated domains (not to scale). **F**, Matrix displays tiling of melanoma tumors (columns) with sequencing available from TCGA and mutations in known

driver genes indicated. **G**, Beeswarm plot shows the nonsynonymous mutation burden (log10) per tumor for MAP3K8 wild-type and rearranged (MAP3K8ΔC) melanoma. **H**, Barplot shows UV-associated mutation (C>T and G>A) frequency in the TCGA melanoma cohort with MAP3K8 altered tumors indicated in red below. **I**, Boxplot shows diagnosis age of patients with wild-type or MAP3K8-rearranged melanomas.

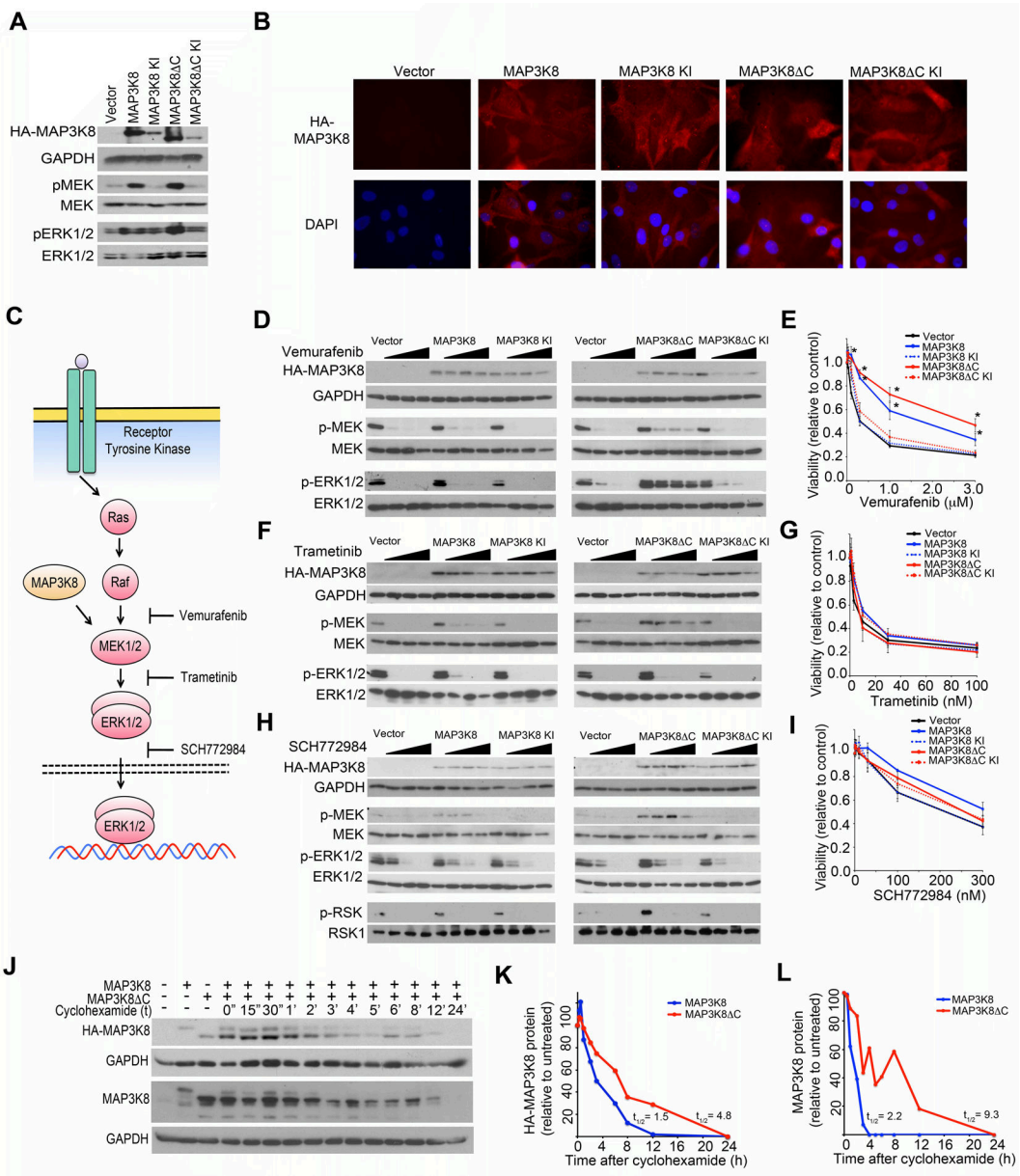

Figure 2. ERK signaling in cells expressing wild type or truncated MAP3K8.

A, Immunoblots show HA-tagged MAP3K8, phospho-MEK1/2, total MEK1/2, phospho-ERK1/2, total ERK1/2 and GAPDH protein levels in 293T cells stably expressing either empty vector, full length MAP3K8, truncated MAP3K8ΔC or kinase inactive (KI) versions. **B**, Images show MAP3K8 localization by immunofluorescence with DAPI nuclear counterstain. **C**, Image depicts MAPK/ERK signaling and inhibitors targeting the pathway. Immunoblots show ERK pathway signaling proteins in cell lines treated with increasing doses of **D**, vemurafenib, **F**, trametinib or **H**, SCH772984. Line graphs display viability of cells treated for 72 h with increasing doses of **E**, vemurafenib (300 nM, 1 μM and 3 μM), **G**, trametinib (1 nM, 3nM and 10 nM) or **I**, SCH772984 (30 nM, 100 nM and 300 nM). **J**, Immunoblot shows HA-tagged MAP3K8, MAP3K8 and GAPDH protein levels in 293T cells 48h after transfection with full-length or MAP3K8ΔC and treatment with

cyclohexamide (100 μg/mL) for indicated timepoints. Line graph show MAP3K8 protein levels over time and half-life ($t_{1/2}$) quantified by densitometry of immunnoblots for **K**, HA and **L**, MAP3K8.

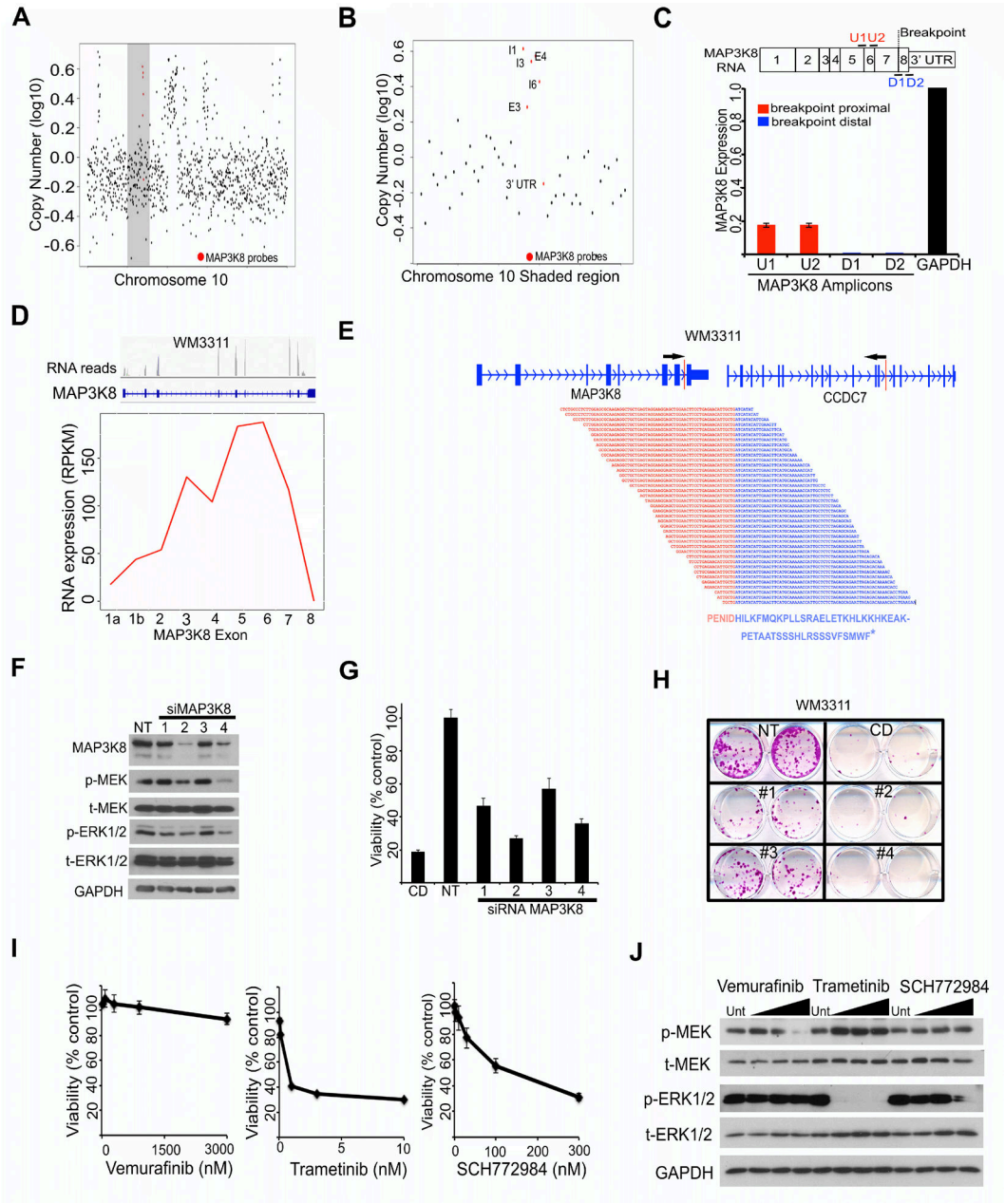

Figure 3. Identification of a melanoma cell line harboring an endogenous MAP3K8 rearrangement.

Scatterplots show **A**, DNA copy number values across chromosome 10 or **B**, zoomed in shaded region (from panel A) with MAP3K8 specific probes indicated in red. **C**, Diagram shows positional qPCR of MAP3K8 transcript from WM3311 cells and expression level discordance between two junction-spanning primers upstream (red) and downstream (blue) of putative breakpoint in MAP3K8. **D**, RNA sequencing read-pileup (top) and exon-level MAP3K8 quantification from WM3311 cells. **E**, Image indicates MAP3K8 breakpoint and breakpoint-spanning sequences from WM3311 cells with resulting protein translation. **F**, Immunoblots show MAP3K8, MEK and ERK1/2 protein levels 72 h after treatment with nontargeting (NT) or four siRNAs targeting MAP3K8 (1–4). **G**, Bar graph shows WM3311

cell viability 72 h after treatment with indicated siRNAs. Cell death (CD) control oligonucleotide indicates transfection efficiency. **H**, Colony forming ability of WM3311 cells after a single reverse transfection of NT, CD and MAP3K8 targeting siRNAs. **I**, WM3311 cell viability and **J**, MAPK/ERK pathway inhibition 72 h after treatment with vemurafenib, trametinib and SCH772984.

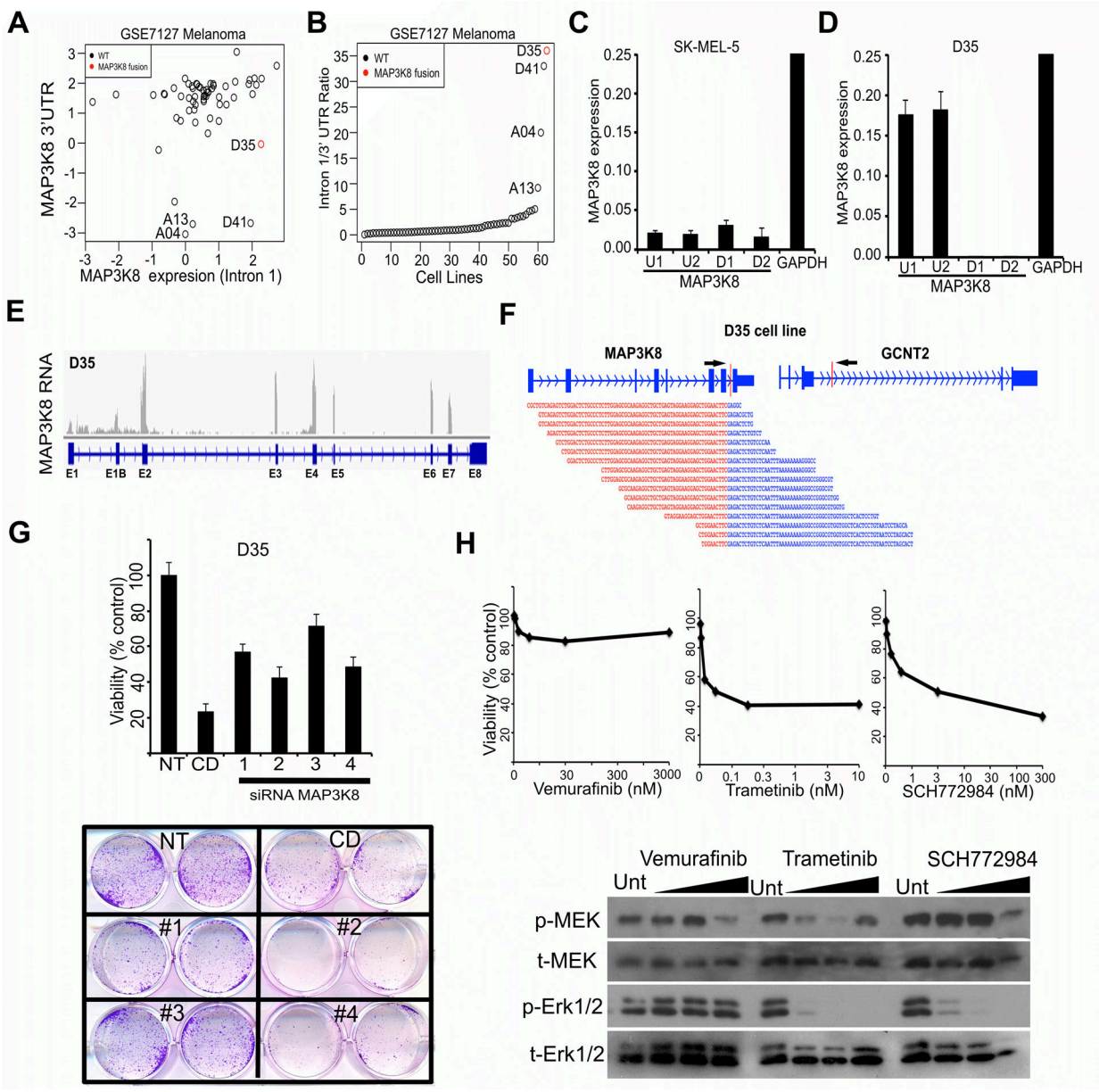

Figure 4. Identification of an additional melanoma cell line dependent on endogenous MAP3K8 rearrangement.

A, Scatterplot show discordant expression in MAP3K8 between intron 1 and 3'UTR of MAP3K8 in a microarray dataset from melanoma cell lines. **B**, Plot shows the ratio of intron1/3' UTR expression across the same datasets with cell lines displaying highest ratio indicated. Positional PCR shows relative expression (qPCR) of MAP3K8 from two amplicons upstream (U1 and U2) and downstream (D1 and D2) of putative MAP3K8 breakpoint in rearrangement negative **C**, SK-MEL-5 and **D**, D35 cells. **E**, RNA-Seq read-pile up shows expression across MAP3K8 coding regions and an absence of reads mapping to exon 8 and 3'UTR of MAP3K8 in D35 cells. **F**, Diagrams shows the orientation MAP3K8 rearrangement identified in D35 cells and breakpoint-spanning reads. **G**, Viability and colony forming ability of D35 cells 72 h after transfection with siRNAs targeting

MAP3K8 or non-targeting (NT) and cell death (CD) controls. **H**, Viability and immunoblot of D35 cells 72 h after treatment with increasing doses of vemurafenib (300 nM, 1 μM and 3 μM), trametinib (1 nM, 3 nM and 10 nM) and SCH772984 (30 nM, 100 nM and 300 nM).

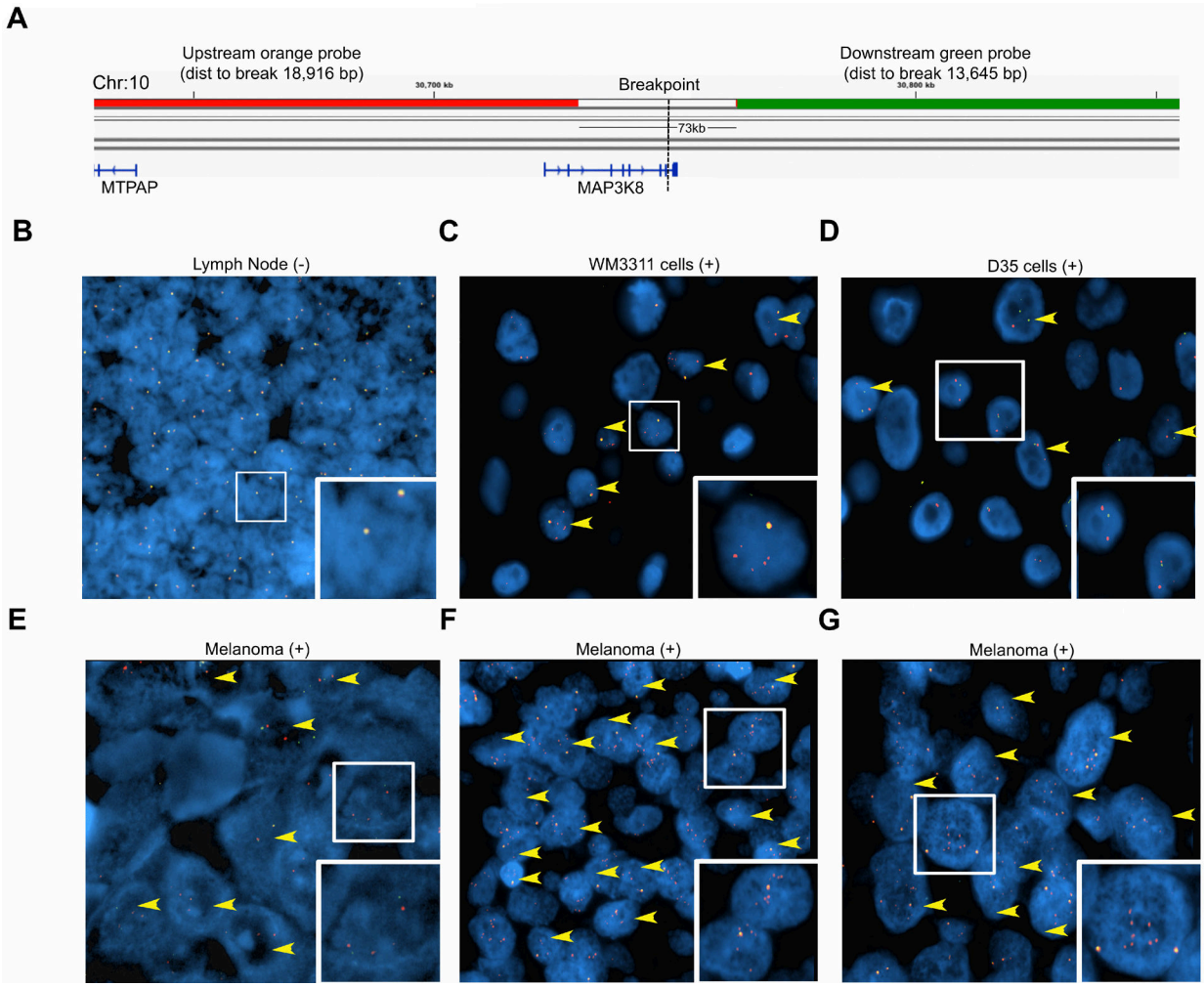

Figure 5. Break-apart FISH strategy identifies MAP3K8 rearrangements and frequency in a melanoma tissue microarray.

A, Image shows fluorescent DNA BAC probes hybridization location with indicated breakpoint distance. Representative FISH images are shown for **B**, lymph node negative control, **C**, WM3311 and **D**, D35 cell lines and **E-G**, human melanomas with MAP3K8 rearrangements. Intact MAP3K8 genomic loci are represented by yellow signal, whereas individual green and orange signals indicate a break. Arrows indicate additional MAP3K8 breakpoint-positive cells.

Table 1.

TCGA Skin Cutaneous Melanoma MAP3K8 Gene Rearrangements

TCGA ID	MAP3K8 Coordinate*	3' Partner Coordinate*	Strand	Split/Span		Copy Number	Histology	Dist. to stop	DNA Region
				RNA	DNA				
TCGA-ER-A196	chr10:30748430	chr20:56937997	(+/−)	1712/707	26/4	Yes	ALM	2	Exonic RAB22A(3' UTR)
TCGA-D3-A2J6	chr10:30748430	chM 0:4473457	(+/+)	100/66	NA/NA	Yes	NOS	19	Intronic ENKUR(I2)
TCGA-EE-A20I	Chr10:30748430	chr10:25344748	(+/+)	695/261	NA/NA	Yes	NOS	9	Intronic GPR98(I85)
TCGA-FR-A20S	chr10:30748430	chr5:90376401	(+/−)	175/82	NA/NA	NA	NOS	5	Exonic LYZL2(E5)
TCGA-FS-A1Z4	Chr10:30748430	chr10:30900953	(+/−)	233/106	NA/NA	No	NOS	44	Intergenic
TCGA-EB-A4IQ	chr10:30748430	chr3:59110263	(+/−)	5/3	NA/NA	Yes	NOS	17	Intergenic

ALM, acral lentiginous melanoma; NOS. not otherwise specified;

*Hg19 alignment coordinates